

Mass spectral characterization of secondary organic aerosol from urban cooking and vehicular sources

Wenfei Zhu¹, Song Guo^{1,2*}, Zirui Zhang¹, Hui Wang¹, Ying Yu¹, Zheng Chen¹, Ruizhe Shen¹, Rui Tan¹, Kai Song¹, Kefan Liu¹, Rongzhi Tang¹, Yi Liu¹, Shengrong Lou³, Yuanju Li¹, Wenbin Zhang⁴, Zhou Zhang⁴, Shijin Shuai⁴, Hongming Xu⁴, Shuangde Li⁵, Yunfa Chen⁵, Min Hu¹, Francesco Canonaco⁶, Andre. S. H. Prévôt⁶

¹ State Key Joint Laboratory of Environmental Simulation and Pollution Control, International Joint Laboratory for Regional Pollution Control, Ministry of Education (IJRC), College of Environmental Sciences and Engineering, Peking University, Beijing 100871, China P. R.

² Collaborative Innovation Center of Atmospheric Environment and Equipment Technology, Nanjing University of Information Science & Technology, Nanjing 210044, China P. R.

³ State Environmental Protection Key Laboratory of Formation of Urban Air Pollution Complex, Shanghai Academy of Environmental Sciences, Shanghai 200233, China P. R.

⁴ State Key Laboratory of Automotive Safety and Energy, Tsinghua University, Beijing 100084, China P. R.

⁵ State Key Laboratory of Multiphase Complex Systems, Institute of Process Engineering, Chinese Academy of Sciences, Beijing 100190, China P. R.

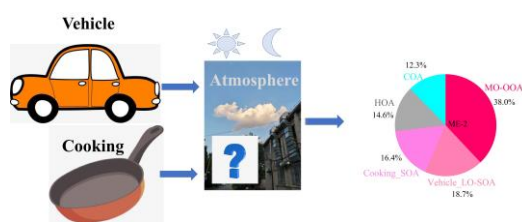
⁶ Laboratory of Atmospheric Chemistry, Paul Scherrer Institute (PSI), Villigen 5232, Switzerland

Corresponding authors:

*Song Guo – State Key Joint Laboratory of Environmental Simulation and Pollution Control, College of Environmental Sciences and Engineering, Peking University, Beijing 100871, China P. R.; Email: songguo@pku.edu.cn

Abstract In the present work, we conducted experiments of secondary organic aerosol (SOA) formation from urban cooking and vehicular sources (cooking and vehicle) to characterize the mass spectral features of primary organic aerosol (POA) and SOA using an high-resolution time-of-flight aerosol mass spectrometer (HR-ToF-AMS). Our results showed that the cooking styles have a greater impact on aged COA mass spectra than oxidation conditions. However, the oxidation conditions affect the aged HOA spectra more significantly than vehicle operation-operating conditions. In our study, we use mass spectra similarity analysis and positive matrix factorization (PMF) analysis to establish the POA and

SOA mass spectra of these two [typical lifestyle](#) sources. These mass spectra are used as source constraints in a multilinear engine (ME-2) model to apportion the OA sources in the atmosphere. Comparing with the traditional ambient PMF results, the improved ME-2 model can better quantify the contribution of POA and SOA from [cooking and vehicular life-style](#) sources. Our work, for the first time, establishes the vehicle and cooking SOA source profiles, and can be further used in the OA source apportionment in the ambient atmosphere.



1. Introduction

Organic aerosol (OA) is an important component of fine particulate matter and has significant environmental and health effects, especially in the urban areas (Guo et al., 2012; Guo et al., 2014; Ying et al., 2020). Currently, real-time measurements of OA based on the aerosol mass spectrometer (AMS) has become an effective way to explore OA characteristics in the field campaigns and laboratory studies (Canagaratna et al., 2007; Ge et al., 2017; Hu et al., 2016a; Huang et al., 2011; Kim et al., 2017; Li et al., 2017; Sun et al., 2016; Zhang et al., 2011). Applying positive matrix factorization (PMF) and a multilinear engine (ME-2) (Paatero, 1999) to analyze the high-resolution mass spectrometry fragments, OA can be further identified as primary organic aerosol (POA) and secondary organic aerosol (SOA). POA includes ~~vehicle exhaust~~ [\(precisely, a kind of hydrocarbon-like OA, \(HOA\), cooking \(COA\), and biomass burning \(BBOA\), which](#) SOA includes low oxygenated OA (LO-OOA) and more oxygenated OA (MO-OOA)(Canonaco et al., 2013; Elser et al., 2016; Qin et al., 2017; Zhang et al., 2017a; Zhou et al., 2018). [Many previous studies have been found that HOA is mainly associated with vehicle-related emissions in the urban atmosphere](#) (Hu et al., 2017; Xu et al., 2016; Zhang et al., 2017a). [Hereinafter, HOA will be referred to as the abbreviation for organic](#)

51 [aerosol emitted by urban vehicles](#). As lifestyle sources in urban, cooking and vehicle emissions, that is COA
52 and HOA mostly determine ambient OA loadings. For example, primary cooking OA (COA) and vehicle
53 exhaust OA (HOA) accounted for 10-35 % and 6-26% of OA, respectively, in urban areas in China (He et al.,
54 2011; Hu et al., 2017; Sun et al., 2010; Sun et al., 2014; Sun et al., 2018; Wang et al., 2016; Xu et al., 2016;
55 Zhang et al., 2014).

56 Besides the contribution to POA, many studies have found that [cooking and vehicular](#) ~~these two typical~~
57 ~~urban lifestyle~~ sources may also emit a large number of volatile organic compounds (VOCs) (Gentner et al.,
58 2009; Katragadda et al., 2010; Klein et al., 2016), semi-volatile organic compounds (SVOCs), and
59 intermediate volatile organic compounds (IVOCs) ($\geq C_{13}$ n-alkanes and fatty acids) (Louvaris et al., 2017;
60 Schauer et al., 2002) ,which may also play important roles in SOA formation. However, based on collocated
61 AMS measurements and factor analysis results, the SOA formed by vehicle and cooking sources cannot be
62 effectively resolved from the total SOA due to the lack of secondary mass spectral profiles. The POA mass
63 spectral profiles based on AMS including HOA (Collier et al., 2015), BBOA (Alfarra et al., 2007; He et al.,
64 2010; Xu et al., 2020), and COA (He et al., 2010; Liu et al., 2017; Mohr et al., 2012; Xu et al., 2020) have
65 been fully explored in laboratory studies, and applied as constraint factors into the ME-2 model in the
66 ambient air. Some studies have made it possible to quantify biogenic secondary aerosol products of a single
67 precursor, such as isoprene oxidation products (IEPOX)(Budisulistiorini et al., 2013; Hu et al., 2016b), and
68 have been extended to the urban atmosphere to obtain an IEPOX-SOA factor via PMF analysis of OA
69 spectra(Zhang et al., 2017b). Although several studies explored the mass spectral characteristics of SOA
70 from [cooking and vehicular](#) ~~anthropogenic life-style~~ sources, i.e., heated cooking oils, gasoline motors, and
71 diesel engines (Kaltsonoudis et al., 2017; Kroll et al., 2012; Liu et al., 2018; Presto et al., 2014), the spectral
72 profiles of cooking SOA under actual cooking conditions and vehicle SOA under different emission
73 conditions are still uncertain. Besides, to date, studies that used ME-2 for a better anthropogenic SOA source

带格式的: 非突出显示

域代码已更改

带格式的: 非突出显示

74 apportionment by inputting their SOA spectra as constraints remain scarce. Therefore, the mass spectra of
75 SOA from abundant cooking and vehicular sources~~anthropogenic life-style sources~~ are urgent to characterize
76 for conducting to acquire a better source apportionment of SOA.

77 In this workstudy, cooking and vehicle experiments were carried out to investigate the variation in ~~mass~~
78 POA and SOA spectra profiles ~~of POA and SOA emitted~~ from vehicle emissions under different running
79 conditions, and Chinese cooking emissions under different cooking styles ~~and vehicle emissions under~~
80 different running conditions using high-resolution time-of-flight AMS (HR-ToF-AMS). The mass spectral
81 characterizations of POA and SOA from cooking and vehicle emissions were intercompared, and their
82 changes in some indicated ionic fragments were elucidated. Besides, we verified the mass spectral profiles
83 by applying ~~mass spectra of~~ POA and SOA profiles to ME-2 for source apportionment of OA in the winter
84 observation with various primary emissions and the summer observation with high oxidation conditions.

85 2. Materials and Methods

86 2.1 Simulation of POA emission and SOA formation from cooking and vehicular ~~urban lifestyle~~ 87 sources.

88 For cooking, we prepared four dishes including deep-frying chicken, shallow-frying tofu, stir-frying
89 cabbage, and Kung Pao chicken. The total cooking time for each experiment ranged from 40 to 66 min,
90 which was almost related to the features of each dish (Table S1). Each dish was continuously carried out 8
91 times in parallel during the cooking process until the closed kitchen was full of fumes. The fumes produced
92 by cooking were introduced through the pipeline from the kitchen into the Gothenburg Potential Aerosol
93 Mass (Go: PAM) reactor (Li et al., 2019) in the laboratory after being diluted 8 times by a Dekati Dilutor
94 (e-Diluter, Dekati Ltd., Finland). Heat insulation cotton was wrapped around the sampling pipelines to
95 prevent fumes from condensing on the wall of the pipe. We considered the emissions sampled after Go:
96 PAM without OH radical as primary emissions, and those ~~measured-monitoring~~ after Go: PAM with ~~the~~

带格式的: 字体: 加粗

97 given OH ~~radicals exposure~~ as secondary formation. The sampling time ranged from 58 to 90 min. Each
98 sampling was in parallel three times. The relative standard deviations were small, which were under 10% in
99 most cases. In addition, the background blank groups and the dilution gas blank groups were separately
100 completed using boiling water and dilution gas, according to the same steps as experimental groups. More
101 information ~~of on~~ experimental setup of cooking simulations ~~can be found~~ has been given in Zhang et al.,
102 2020_-(Zhang et al., 2020).

103 For vehicle, experiments were performed by using Gasoline direct engine (GDI)~~engine~~ with a
104 commercial China V gasoline fuel (Emission: 998cc; Maximum power: 100KW 6000rpm; Peak torque:
105 205Nm 2000-3000rpm). Vehicle operating under real-life conditions were dynamic rotating speed-torque
106 combination. For example, the combination of 1500 rpm rotating speed and 16Nm torque, 2000rpm, and
107 16Nm torque for the engine in this study reflect the realistic vehicle speed of 20km/h and 40km/h,
108 respectively. Five running conditions covering different speeds and torques, including 1500rpm_16Nm,
109 1750rpm_16Nm, 2000rpm_16Nm, 2000rpm_32Nm, and 2000rpm_40Nm, were used to characterize their
110 POA and SOA mass spectra in this study. Once the engine warmed up, it continued to work under one
111 running condition. After the three-way catalytic system, the exhaust from the engine tailpipe was diluted 30
112 times by the same dilution system for the cooking experiment. Then the diluted exhaust entered the Go:
113 PAM through the stainless pipe wrapped by heat insulation cotton. For each running condition, five parallel
114 experiments were conducted (Table S2). The sampling time with collecting three parallel data groups was
115 about 60 min for each experiment. ~~We adjusted input ozone concentration ranging from 0 to 7.7 ppm to~~
116 ~~change the OH exposure in the Go: PAM.~~

117 Go: PAM reactor consists of quartz tube that is 100 cm long and 9.6 cm in diameter, as described in
118 Watne et al., 2018 (Watne et al., 2018). The OH radicals in Go: PAM reactor is generated by the photolysis
119 of ozone and the reaction in the presence of water vapor. ~~We adjusted input ozone concentration ranging~~

带格式的: 字体: 加粗

from ~0 to ~7.76.5 ppm and ~0 to ~4.0 ppm to change the OH exposure radicals in the Go: PAM for vehicle and cooking experiments, respectively. The temperature, relative humidity, and the sampling residence time in Go: PAM for vehicle and cooking experiments were documented in the supplement material (Table S3).

带格式的: 字体: 加粗

2.2 Instrumentation and data analysis.

Figure S1 shows the design drawing on schematic vehicle and cooking experiments of the experimental system is presented in Figure S1. Two scanning mobility particle sizers (SMPS 1, Electrostatic Classifier model 3080, Condensation Particle Counter model 3778; SMPS 2, Electrostatic Classifier model 3082, Condensation Particle Counter model 3772; TSI Incorporation, USA) were set at the inlet and outlet of Go: PAM to correct the wall loss (Zhang et al., 2020). The size distribution and number concentration of particles were scanned every 2 (cooking) - 5 min (vehicle) before and after Go: PAM for cooking and vehicle experiment, respectively. The chemical compositions, mass concentrations of non-refractory submicron aerosol (NR-PM₁), and high-resolution ions fragments of OA were measured recorded by an aerodyne high resolution time of flight aerosol mass spectrometer (HR-ToF-AMS, (Aerodyne Research Incorporation, USA), synchronize with SMPS.

带格式的: 下标

Before and after the two experiments, the ionization efficiency (IE) of HR-ToF-AMS IE calibrations were carried out calibrated by using applying 300 nm mono-dispersed ammonium nitrate particles synchronization combining with SMPS. The collection efficiency (CE) of HR ToF AMS was obtained from comparing AMS and synchronous SMPS real-time measurement of particle mass concentrations at the outlet of Go: PAM. Besides, the real-time measurements of CO₂ concentrations (Model 410i, Thermo Electron Corporation, USA) were simultaneously measured used using a CO₂ analyzer (Model 410i, Thermo Electron Corporation, USA) to reduce correct the influence of CO₂ interference to on organic OA ion fragments, refer to Canagaratna et al., 2015 (Canagaratna et al., 2015) in mass spectra. Other gas phase measurements included carbon monoxide (CO, Thermo, Model 48i TL), NO_x (Thermo, Model 42i TL), and SO₂ (Thermo,

带格式的: 非突出显示

带格式的: 非突出显示

带格式的: 非突出显示

带格式的: 非突出显示

带格式的: 非突出显示

带格式的: 非突出显示

带格式的: 非突出显示

带格式的: 非突出显示

域代码已更改

带格式的: 非突出显示

143 Model 42i TL).

144 The mass concentration, size distribution, and the ion-specified mass spectra of NR-PM₁ species were
145 analyzed using the HR-ToF-AMS standard data analysis software (SQUIRREL version 1.57 and PIKA
146 version 1.16). ~~In this study, we used the Igor-based PMF model with PMF2.exe algorithm (Paatero and
147 Hopke, 2003) and the PMF Evaluation Toolkit version 2.08D (Ulbrich et al., 2009) to separate the POA and
148 SOA from aged cooking and vehicle organic aerosol, following the procedure presented in the literatures
149 (Hu et al., 2016a; Zhang et al., 2011). The elemental compositions (O/C, H/C, N/C, and OM/OC) were
150 estimated by the “improved-ambient” updated method (Canagaratna et al., 2015). The OH exposure and
151 equivalent photochemical age (EPA) were calculated by off-line methods according to SO₂ decay shown in
152 Zhang et al., 2020 (Zhang et al., 2020), which were validated by a flow reactor exposure estimator using
153 measured concentrations of reactive compounds such as VOCs, CO₂ and NO_x (Peng et al., 2016). The OH
154 exposure and photochemical age for all conditions in cooking and vehicle experiments were listed in **Table**
155 **S1S3**.~~

156 **2.3 OA source apportionment**

157 The PMF model can describe the variability of a multivariate database as a linear combination of static
158 factor profiles and their corresponding time series (Huang et al., 2020; Wang et al., 2017; Zhu et al., 2018).
159 In this study, we used the Igor-based PMF model with PMF2.exe algorithm (Paatero and Hopke, 2003) and
160 the PMF Evaluation Toolkit version 2.08D (Ulbrich et al., 2009) to split POA and SOA factors from cooking
161 and vehicle aged OA. The PMF model was also used to identify the source of OA for ambient atmosphere
162 during the summer and winter observations of Shanghai, following the procedure presented in the literature
163 (Hu et al., 2016a; Zhang et al., 2011), as described in section 3.3. In contrast to an unconstrained PMF
164 analysis, ME-2 algorithm allows the user to add prior information (e.g., source profiles) into the model to
165 constrain the matrix rotation and separated the mixed solution. In this study, we adopted the toolkit SoFi

带格式的: 字体: 加粗

带格式的: 字体: 加粗

(Source Finder) within a-value approach to perform organic HR-AMS datasets collected in Shanghai. The a-value can vary between 0 and 1, which is the extent to which the output profiles can vary from the model inputs. The a-value test was performed following the technical guidelines presented in Crippa et al. (2014) (Crippa et al., 2014). The reference mass spectral profiles that constrained in ME-2 analysis were derived from lab-based primary and secondary cooking and vehicular factors of this study. Details of the algorithm could refer to previous studies (Canonaco et al., 2013; Huang et al., 2020; Reyes-Villegas et al., 2016).

2.3 2.4 Mass spectra similarity analysis.

In this study, the angle θ was used to evaluate the correlation between the two AMS mass spectra features. The angle θ between the two AMS mass spectra (MSa, MSb) is given by:

$$\cos\theta = \frac{MSaMSb}{|MSa||MSb|}$$

The θ angle between two mass spectra is 0-5, 5-10, 10-15, 15-30, and > 30 , which means excellent consistency, good consistency, many similarities, limited similarities, and poor consistency, respectively, (Kaltsonoudis et al., 2017; Kostenidou et al., 2009).

3. Results and Discussion

3.1 Mass spectra of POA and aged OA from the ~~cooking and vehicular sources~~ life style sources.

Fig.1a shows the mass spectra of aged HOA under different vehicle running conditions when EPA was 0.6 days. The mass spectra of aged HOA emission from different vehicle running conditions under other various oxidation degrees are included in **Fig.S2**. All the aged HOA spectral profiles from different vehicle running conditions showed a similar pattern, and the θ angles among the mass spectra of aged HOA were less than 10° at EPA 0.6 days (**Table 1**), suggesting a little difference between the mass spectra. The mass spectra of aged HOA at 0.6 days were dominated by the ion series of $C_nH_{2n+1}^+$ (m/z 29, 43, 57, 71, 85...) and $C_nH_{2n-1}^+$ (m/z 41, 55, 69, 83...), resulting from less oxidized components such as saturated alkanes, alkenes. As the highest proportion of ion fragments, m/z 43 and 29 consisted of oxygen-containing ions like CHO^+

带格式的: 正文, 无项目符号或编号

带格式的: 字体: (默认) Times New Roman, 小四, 加粗

189 and $C_2H_3O^+$, respectively, whose fractions were much larger than the hydrocarbon-like ion fragments at the
190 same mass integers. Besides, there were also abundant tracer ion fragments for SOA (m/z 28 and m/z 44).

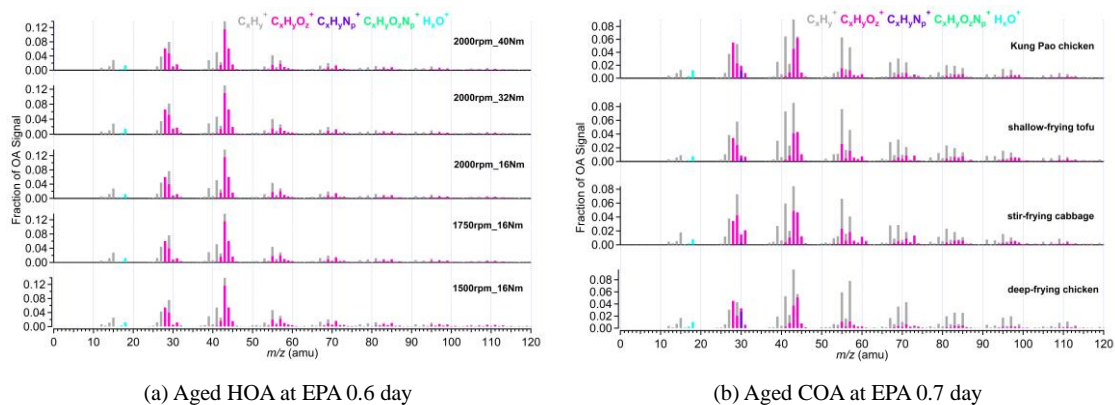


Fig.1. (a) The mass spectra of aged HOA emission from different vehicle running conditions at EPA 0.6 day; (b) The mass spectra of aged COA from four Chinese dishes at EPA 0.7 day. Five running conditions covers different speeds and torques, including 1500rpm_16Nm, 1750rpm_16Nm, 2000rpm_16Nm, 2000rpm_32Nm, and 2000rpm_40Nm. Four dishes include deep-frying chicken, shallow-frying tofu, stir-frying cabbage, and Kung Pao chicken.

191

192 The mass spectra of aged COA at 0.7 days of EPA are presented in **Fig.1b**. Detailed mass spectra of
193 aged COA under other various oxidation degrees are included in **Fig.S3**. The similarity of aged COA among
194 different types of cooking were was greater than that of aged HOA among different running conditions when
195 the EPA was at the same level. Except for the θ angles of deep-frying chicken vs stir-frying cabbage (21°),
196 and deep-frying chicken vs shallow-frying tofu (19°), the θ angles among other aged COA at EPA 0.7 day
197 exhibited good agreement ($\theta < 15^\circ$) in mass spectra (**Table 1**). The mass spectra of cooking were dominated
198 by the similar ion series as those of vehicle, which were mostly m/z 28, m/z 29, m/z 41, m/z 43, m/z 44, m/z
199 55, m/z 57, m/z 67, and m/z 69. However, the major mass spectral differences between cooking and vehicle
200 were the abundance of m/z 41 and the ratio of oxygen-containing ions to hydrocarbon ions ($C_xH_yO_z^+/C_xH_y^+$).
201 The four Chinese dishes had prominent peaks at m/z 41, m/z 43, and m/z 55 (generated from $C_3H_5^+$ and
202 $C_3H_7^+$, $C_4H_7^+$) which was qualitatively consistent with mass spectra of primary COA in other studies (Xu et
203 al., 2020). As described by [He et al. \(2010\)](#) [He et al., 2010](#), the most abundant ion fragments at m/z 41 and

m/z 55 from primary Chinese cooking emissions [associated with frying](#) are resulting from unsaturated fatty acids ([He et al., 2010](#)).

域代码已更改
带格式的: 非突出显示

Table 1 The θ angles among the mass spectra of (a) aged HOA at EPA 0.6 day and (b) aged COA at EPA 0.7 day

(a) θ angles	1500rpm_16Nm	1750rpm_16Nm	2000rpm_16Nm	2000rpm_32Nm	2000rpm_40Nm
1500rpm_16Nm	0	3	3	8	4
1750 rpm_16 Nm		0	0.1	5	3
2000 rpm_16 Nm			0	5	3
2000 rpm_32 Nm				0	4
2000 rpm_42 Nm					0

(b) θ angles	deep-frying chicken	stir-frying cabbage	shallow-frying tofu	Kung Pao chicken
deep-frying chicken	0	21	19	14
stir-frying cabbage		0	10	13
shallow-frying tofu			0	12
Kung Pao chicken				0

Fig.2a shows the mass spectra of aged HOA oxidation at different OH exposures under the same vehicle running condition (2000rpm, 16Nm). The changes in mass spectra of aged HOA under different conditions are provided in **Fig.S4**. [It was worth noting that the source characteristics of vehicle POA were uncertain due to its low concentration emitted from the engine in this study. A related study has found that the POA factor from vehicle emissions is similar to the HOA factor derived from environmental datasets \(Presto et al., 2014\). Therefore, we used the average HOA spectrum derived from unconstrained PMF analysis based on the ambient observations of Shanghai, Beijing, Dezhou, Shenzhen in China as an alternative to the mass spectrum of vehicle POA, as shown in Fig.2a and Fig S4. Detailed observation information of Shanghai, Dezhou, and Shenzhen referred to Zhu et al., 2021\(Zhu et al., 2021a\). The observations in Beijing have been given in \(Hu et al., 2017\).](#) The HOA spectrum was similar to that reported

in (Ng et al., 2011), which has been widely used as traffic emission profiles. As the oxidation degree increased, the ion fragments varied similarly with hydrocarbon-like ion fragments decreasing. The mass spectra at 2.89 days and 4.15 days had very similar patterns with the most prominent abundant signals peaks at m/z 28 and 44, respectively (Fig.2 and Fig.S4), which almost resembled showed good consistency with the mass spectra of MO-OOA resolved from ambient datasets ($\theta = 14^\circ$; compared with MO-OOA obtained during the spring observations in Zhu et al., 2021b) (Ng et al., 2011; Zhu et al., 2021b). When EPA was 1.65 7 days, there were different mass spectra patterns, with dominant signals at m/z 28 and m/z 44, yet contained a large signal at m/z 43, similar to many similarities with the spectra of the ambient LO-OOA (Fig.2 and Fig.S4) (Hu et al., 2017; Zhu et al., 2021b). Oxidation degrees greatly affected the similarity of mass spectra between POA and those of aged HOA. The mass spectra profile of vehicle POA-HOA ambient displayed poor agreement ($\theta > 30^\circ$) with all aged HOA spectra profiles (Tables S4-S56). Besides, the mass spectra under the low oxidation degree (EPA was 0.6 day) was also poorly correlated with those mass spectra under the high oxidation degree (EPA were 2.89 and 4.15 days) (Table S6).

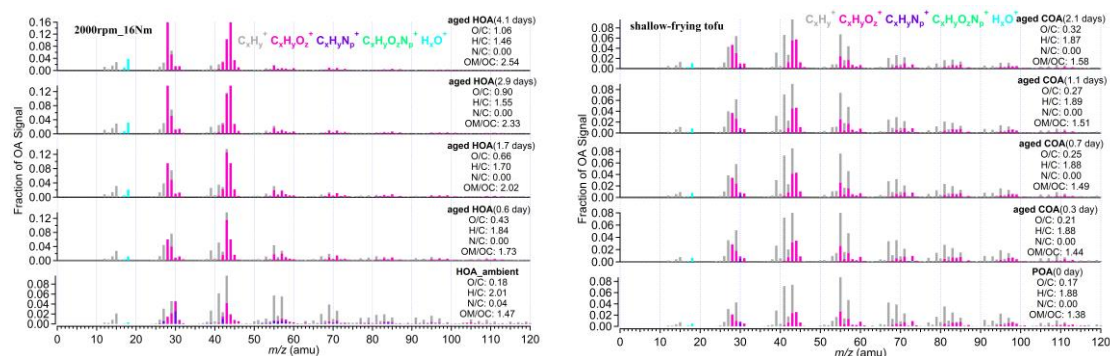


Fig.2. (a) The mass spectra of HOA and aged HOA oxidation of under four different OH exposure under at the same vehicle emission running condition (2000rpm, 16Nm). (b) The mass spectra of primary COA and aged HOA-COA oxidation of different OH exposure for shallow-frying tofu. The OH exposure and equivalent photochemical age (EPA) were calculated by obtained from off-line methods according to SO_2 decay shown in Table S4S3. The elemental compositions were estimated by the "improved-ambient" updated method (Canagaratna et al., 2015).

The mass spectra of primary COA primary COA and aged COA showed great inter-correlations ($\theta <$

带格式的: 字体: 加粗

带格式的: 字体: 加粗

带格式的: 字体: 加粗

带格式的: 字体: 加粗

带格式的: 字体: 加粗

15 %), which were smaller than that of vehicle OA (Table S4-S5S7). ~~Along with the growth of OH exposure, the f_{43} of aged COA increased from 0.07 to 0.10, and meanwhile its f_{44} increased from 0.03 to 0.08 (Fig.2b; Fig.S5), distributing in the lower region of less oxidized organic aerosol (LO-OOA).~~ The spectra of these aged COA derived herein displayed ~~almost the same variation~~ good consistency with those ~~of from~~ cooking oils ~~OA~~ (Liu et al., 2018) (Fig.2b and Fig.S5). It should be noted that the fractions of m/z 28 and m/z 44 signals in aged COA were lower than those of aged HOA at the similar EPA. In addition, the aged COA had more hydrocarbon-like ions at the same mass integers than aged HOA.

All the above results imply that oxidation condition drives the variabilities in mass spectra of the vehicle OA. In contrast, cooking styles instead of oxidation conditions, significantly affected the mass spectra of cooking OA. Here we concluded some possible explanations for these results. On one hand, under the same oxidation conditions and different emission conditions, the similarity among the mass spectra of vehicles was larger than that of cooking, which may be related to their precursors. Some studies have shown that the species and the proportion of gaseous organic matter emitted by different dishes are quite different (Wang et al., 2018). As described in the literature, alkanes and oxygenated volatile organic compounds (O-VOCs) contributed to over 97% of the total VOCs for fried food, and O-VOCs were the dominant contributors for Sichuan and Hunan cuisine where stir-frying is common (Wang et al., 2018). Different gaseous precursors cause distinctions in the particle phase SOA formation, which is reflected in the variations of AMS ion fragments between four dishes in our study. Compared to cooking, the precursors from vehicles are mainly hydrocarbons, and the difference in emissions under different running conditions is inapparent (Robinson et al., 2007). On the other hand, under the same emission conditions and different oxidation conditions, the similarity among the mass spectra of cooking sources is larger than that of vehicle sources, likely due to the oxidation pathway of precursors. As mentioned above, O-VOCs are important precursors of cooking sources, and their oxidation mechanisms ~~is-are~~ mostly alcohol/peroxide substitution

带格式的: 字体: 加粗

带格式的: 字体: 加粗

258 process. This conclusion was proved by a Van Krevelen diagram, showing that the cooking data gather
259 around the slope of approximately -0.1 (Zhang et al., 2020), in agreement with that of heated oils OA (Liu et
260 al., 2018). However, for vehicles, with the increase of oxidation degrees, the reaction pathways of
261 hydrocarbon precursors varied diversely. In Van Krevelen space, the vehicle data fell along a line with a
262 slope of -0.5 (Fig.S6), indicating oxidation processes involving the addition of both carboxylic acid and
263 alcohol or peroxide functional groups without fragmentation and/or the addition of carboxylic acid
264 functional groups with fragmentation.

3.2 Identification of the cooking and vehicular sources ~~life-style sources~~ SOA mass spectra.

266 Although the f_{44} (proportion of m/z 44 in OA) of aged COA raised from 0.03 to 0.08 with oxidation
267 increasing (Fig.2b and Fig.S5). The-the high abundance of m/z 41, 55, and 57 in aged COA mass spectra for
268 four dishes may be a sign that aged OA identified in this study is a mixture of POA and SOA. PMF analysis
269 was performed on the high-resolution mass spectra to split SOA and POA factors from aged COA under
270 each dish. Similarly, the same PMF procedure was also applied for vehicle datasets for each running
271 condition. The choice of the PMF solution can be found in the supplement material (Fig.S7-S10 and Table
272 S8-S9; taken stir-frying cabbage for cooking, and 2000rpm_32Nm for vehicle as an example).

273 Some ions like m/z 41, 55, 57, 43, 28, and 44 are typically used as tracers of OOA, COA, HOA,
274 LO-OOA, and MO-OOA. Fig.3 shows the high-resolution mass spectra of POA and SOA from four Chinese
275 dishes and five vehicle running conditions. The cooking PMF POA of four Chinese dishes all showed
276 obvious hydrocarbon-like ~~features with a large abundance of f_{57} , f_{55} or f_{41} (fraction of signals at m/z 57, 55~~
277 ~~and 41 in OA, respectively)~~ 41, 43, 55, and 57 with ion fragments of $C_3H_5^+$, $C_3H_7^+$, $C_4H_7^+$, $C_4H_9^+$, $C_5H_7^+$ and
278 $C_5H_9^+$. ~~For all experiments, the fraction of prominent peaks of cooking POA were~~ m/z 41 in cooking POA
279 ranged from ($f_{41}=0.051$ to -0.069), —The prominent fraction of m/z 43 ($f_{43}=0.068\sim 0.083$), 55
280 ($f_{55}=0.064\sim 0.084$), 57 ($f_{57}=0.041\sim 0.097$), 67 ($f_{67}=0.021\sim 0.40$), 69 ($f_{69}=0.034\sim 0.049$) were observed (Table

带格式的: 字体: 非加粗

带格式的: 字体: 加粗

带格式的: 字体: 加粗

带格式的: 非突出显示

带格式的: 非突出显示

带格式的: 非上标/下标

带格式的: 非突出显示

带格式的: 非突出显示

带格式的: 非突出显示

带格式的: 非突出显示

带格式的: 非突出显示

带格式的: 非突出显示

带格式的: 字体: 加粗

~~S10), dominated by $C_3H_5^+$, $C_3H_7^+$, $C_4H_7^+$, $C_4H_9^+$, $C_5H_7^+$ and $C_5H_9^+$ respectively. It was observed that fractions of oxygen-containing ions were rising while those of hydrocarbon-like ions were declining during the oxidation process. As for mass spectra of cooking SOA, the fractions of For mass spectra of cooking PMF SOA, the oxygen-containing oxidation ions fragments were had higher signals than those of hydrocarbon-like ion fragments. The prominent dominate signals existed at peaks were m/z 28 ($f_{28}=0.045\sim0.068$), 29 ($f_{29}=0.048\sim0.080$), 41 ($f_{41}=0.050\sim0.068$), 43 ($f_{43}=0.087\sim0.103$), 44 ($f_{44}=0.058\sim0.080$), 55 ($f_{55}=0.050\sim0.064$) (Table S11), and 57 ($f_{57}=0.036\sim0.067$), dominated by CO^+ , CHO^+ , $C_2H_5^+$, $C_3H_7^+$, $C_2H_3O^+$, CO_2^+ , $C_3H_5^+$, $C_4H_7^+$, $C_3H_3O^+$, $C_4H_9^+$ and $C_3H_5O^+$ respectively. The evolution of m/z 43 from POA to SOA revealed a larger fraction and enhancement than those of m/z 44, suggesting that the domestic cooking SOA may generate from a less oxidized process.~~

Different from the cooking, ~~two two-vehicle PMF~~ SOA factors were derived from ~~vehiele SOA-aged HOA~~ due to higher OH exposure. According to different O/C ratios, they were considered to be low oxidized vehicle SOA (LO-SOA) and more oxidized vehicle SOA (MO-SOA). As indicated in **Fig.3** and **Table S12**, the prominent m/z 28 (average $f_{28}=0.045$), 41 (average $f_{41}=0.046$), 43 (average $f_{43}=0.158$), 44 (average $f_{44}=0.054$), 55 (average $f_{55}=0.039$), 57 (average $f_{57}=0.027$) of PMF LO-SOA were comparable with those of cooking PMF SOA. The fraction of m/z 43 of PMF LO-SOA was higher than that in cooking SOA by a factor of 2. The abundant m/z 28 and 44 (mainly generated from CO_2^+) are widely used as the ambient MO-OOA markers. (Sun et al., 2018; Xu et al., 2017). We observed high fractions of m/z 28 ($f_{28}=0.110\sim0.214$) and m/z 44 ($f_{44}=0.121\sim0.224$) in PMF MO-SOA (Table S13) and high O/C ratios (0.88~1.33), which were much higher than those of PMF LO-SOA (O/C=0.37~0.53) and cooking SOA (O/C=0.29~0.41).

带格式的: 非突出显示

带格式的: 非突出显示

带格式的: 非突出显示

带格式的: 非突出显示

带格式的: 非突出显示

带格式的: 非突出显示

带格式的: 字体: 非加粗

带格式的: 字体: 加粗

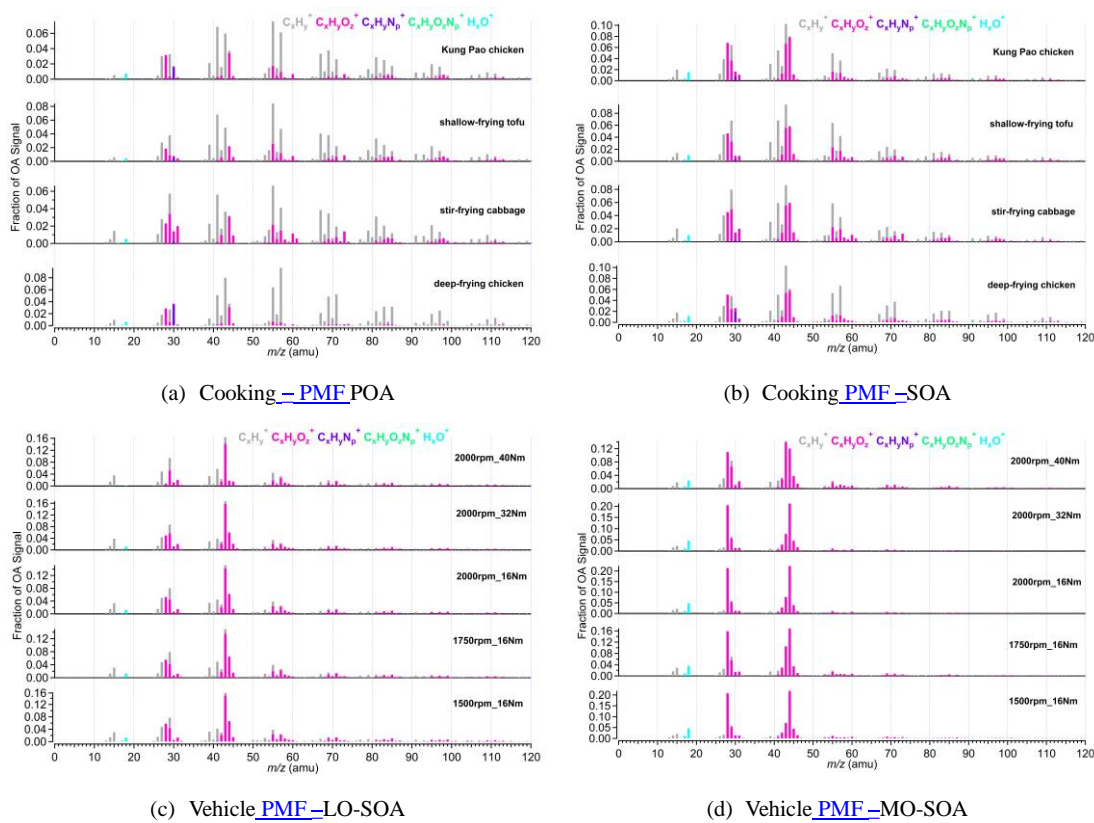


Fig.3. The mass spectra of PMF-POA_s and SOA from vehicle and cooking. PMF analysis was performed on the high-resolution mass spectra to split two factors (cooking POA and SOA) from aged COA and two SOA factors (vehicle LO-SOA and MO-SOA) from aged HOA, respectively.

Similarly, for the resolved SOA factors, the correlation of mass spectra among cooking groups under different cooking methods ($\theta = 8\sim 21^\circ$) was worse than that of vehicle groups (LO-SOA; $\theta = 3\sim 719^\circ$) under different running conditions (**Table S8S14**; **Table S40S16**). The mass spectra of the PMF POA factors for deep-frying chicken exhibited poor agreement with those of stir-frying cabbage, Kung Pao chicken, and shallow-frying tofu (**Table S9S15**). In addition, we also found that the θ angles between LO-OOA-SOA and MO-OOA-SOA under five GDI running conditions were ranged from 36° to 50° (**Fig.S7S11**), indicating that the mass spectra profiles of PMF LO-OOA-SOA are ~~much different~~poor consistency with ~~from~~ those of PMF MO-SOA, consistent with the changes in the mass spectra characteristics of vehicles, under the

311 same emission conditions and different oxidation conditions. Our results suggest that it is necessary to
312 consider the cooking styles when constraining cooking and atmospheric oxidation conditions when
313 constraining vehicle factors.

314 **3.3 Application of established POA and SOA profile in ambient OA source apportionment.**

315 ~~Based on the similarity analysis results of the four cooking groups, the mass spectra of deep frying~~
316 ~~chicken were poorly correlated with the others. Therefore, taking into account the cooking methods of~~
317 ~~Chinese dishes, PMF model was used to identify t~~The POA and SOA of the cooking as the primary and
318 secondary spectrum constraints for ME-2 ~~were obtained~~ by ~~combining-averaging~~ the high-resolution mass
319 spectra datasets of the ~~three-four~~ dishes, ~~which were identified from aged COA using PMF model, except for~~
320 ~~deep frying chicken~~. Similarly, combining different GDI running conditions, ~~the averaged~~ LO-SOA and
321 MO-SOA which were resolved based on ~~aged HOA by using the~~ PMF model were used as the inputting
322 mass spectra profiles of vehicles for ME-2. ~~The mass spectral profiles for cooking and vehicle as constraints~~
323 ~~in ME-2 model are shown in (Fig.S8S12).~~

324 The θ angles between the mass spectral profiles from urban ~~cooking and vehicular sources~~~~lifestyle~~
325 ~~sources~~ and ambient PMF-resolved factors were calculated and summarized in **Fig.4** and **Table S4S18**. The
326 AMS mass spectra of ambient factors were obtained ~~and averaged~~ in Shanghai, Dezhou, Beijing, and
327 Shenzhen in China (Hu et al., 2017; Zhu et al., 2021a). The θ angles among ambient COA, HOA, LO-OOA
328 and MO-OOA factors and the cooking ~~PMF~~-POA, SOA, and the vehicle ~~PMF~~-LO-SOA, MO-SOA were
329 ranged from 18° to 52° (**Fig.4**), suggesting that the cooking ~~PMF~~-POA, SOA, and the vehicle ~~PMF~~
330 LO-SOA, MO-SOA can be used as source constraints for ME-2 in ambient air.

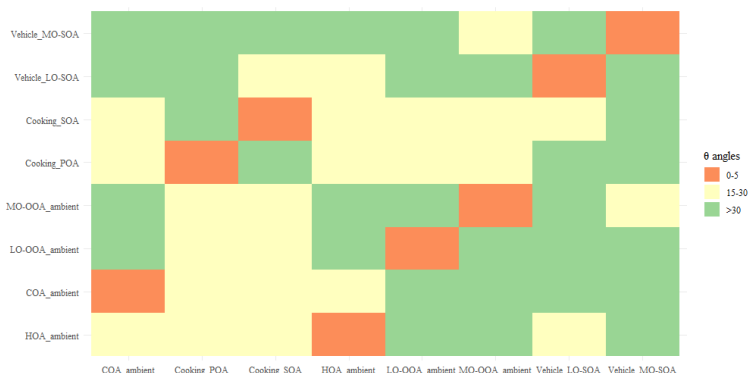


Fig.4. The θ angles between ambient COA, HOA, LO-OOA, and MO-OOA factors and the cooking PMF POA, SOA, and the vehicle **PMF**-LO-SOA, MO-SOA. The θ angle between two mass spectra is 0-5, 5-10, 10-15, 15-30, and > 30 indicates excellent consistency, good consistency, many similarities, limited similarities, and poor consistency, respectively. [The ambient COA, HOA, LO-OOA, and MO-OOA factors were averaged the resolved factors which performed on Shanghai, Dezhou, Beijing, and Shenzhen datasets](#) (Hu et al., 2017; Zhu et al., 2021a).

331 ~~the maximum SOA potential would occur over an ambient timescale less than 1–1.5 days. Constraining~~
 332 ~~many SOA factors could be over-constraining the ME-2 runs, which leads to factor mixing and reduces the~~
 333 ~~number of factors. In addition, Considering considering the actual oxidation conditions or, that is the~~
 334 ~~concentration of OH radicals, and the lacking vehicle POA, the cooking **PMF**-POA, cooking SOA, and the~~
 335 ~~vehicle **PMF**-LO-SOA, and ambient HOA (instead of vehicle POA; derived from Beijing, Shenzhen,~~
 336 ~~Dezhou, Shanghai ambient measurements)~~ was finally selected as the input source spectra of ME-2. We
 337 further demonstrated the feasibility of input primary and secondary mass spectra for OA source
 338 apportionment in two field campaigns at urban site of Shanghai in summer and winter. [The ambient](#)
 339 [measurements in Shanghai were taken in situ at the same location as \(Zhu et al., 2021a\), i.e., Shanghai](#)
 340 [Academy of Environmental Sciences \(31.10°N, 121.25°E\), a typical urban site in the Yangtze River Delta](#)
 341 [region from 23 August to 5 September 2016, and from 28 November 2016 to 12 December 2017 with](#)
 342 [HR-ToF-AMS at 4 min time resolution. In addition, In general, the ME-2 source analysis was performed by](#)
 343 [using constraining two primary OA factors \(the cooking **PMF**-POA, HOA-resolved in three cities\) and two](#)
 344 [secondary OA factors \(the cooking **PMF**-SOA, the vehicle **PMF**-LO-SOA\) as constraints with the fixed](#)
 345

带格式的: 非突出显示

a-value of 0.1 for HOA, 0.2 for cooking POA, 0.4 for vehicle LO-SOA and cooking SOA based on the same ambient OA datasets as PMF model during the summer and winter observations of Shanghai. In ME-2 solutions from 1 to 7 factors, we found the solution of 6 factors (i.e., COA, HOA, Other-POA, Cooking SOA, Vehicle LO-SOA) was most interpretable for the wintertime observations. For the 5 factors solution, in addition to the constraint four factors, factor 5 appeared to be mixed primary and secondary features. However, Other-POA split into two factors with similar profiles in seven factors solution (Fig.S13). Source apportionment on OA datasets by using the unconstrained PMF model was also examined to compare with ME-2 analysis. The choice for the optimal solution for the PMF model was presented in the supporting information (Fig.S14-S16 and Table S19-S20). Ambient PMF-resolved OA factors included POA factors (i.e., HOA, COA), and SOA factors i.e., LO-OOA and MO-OOA (oxygenated OA) in the summer and winter observations in Shanghai, on average accounting for 27%, 35%, and 38% of OA mass. OOA resolved by PMF model did not separate into two types of OOA including LO-OOA and MO-OOA. Besides, we observed that HOA and COA profiles (provided via PMF during the wintertime) contained high signals at the biomass burning tracer ion (m/z 73), and m/z 91 (PAH-related m/z), indicating that the mixing among HOA, COA, and other POA (e.g., BBOA) (Figure 5).

~~Ambient PMF-resolved OA factors included POA factors i.e., HOA, COA, and SOA factors i.e., LO-OOA and MO-OOA in the summer and winter observations in Shanghai. The HOA and COA identified by PMF contributed as high as 16 % and 26 % to OA in the winter observation, respectively, far exceeding expectations (Fig.5). In addition, the ME-2 source analysis was performed by using two primary OA factors (the cooking PMF POA, HOA resolved in three cities) and two secondary OA factors (the cooking PMF SOA, the vehicle PMF LO-SOA) as constraints based on the same ambient OA datasets as PMF model during the summer and winter observations of Shanghai.~~

带格式的: 字体: 加粗

带格式的: 字体: 加粗, 非突出显示

带格式的: 字体: 加粗

带格式的: 字体: 加粗

带格式的: 字体: 加粗, 非突出显示

带格式的: 字体: 加粗

带格式的: 字体: 加粗, 非突出显示

带格式的: 字体: 加粗, 非突出显示

带格式的: 字体: 加粗

带格式的: 字体: 加粗, 非突出显示

带格式的: 字体: 加粗

带格式的: 字体: 加粗, 非突出显示

带格式的: 字体: 加粗

带格式的: 字体: 加粗, 非突出显示

带格式的: 字体: 加粗

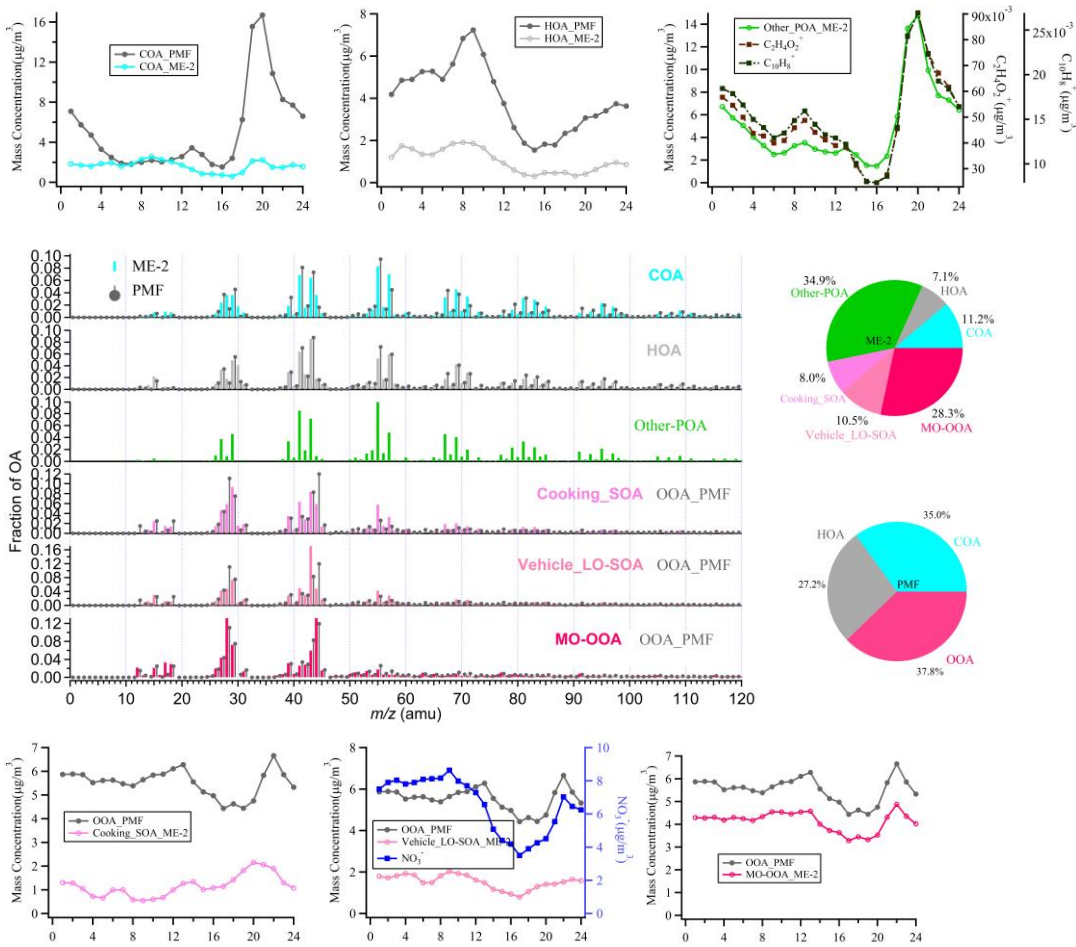


Fig.5. The comparison of the mass spectra, the diurnal variation, and fraction between ME-2 and PMF resolved factors during the wintertime in Shanghai. The black lines in the spectra and diurnal pattern are the result of PMF analysis of the actual atmosphere in Shanghai winter. The others correspond to the ME-2 source analysis results by using two primary OA factors (the cooking ~~PMF~~ POA, ~~ambient HOA-resolved-in-three-cities~~) and two secondary OA factors (the cooking ~~PMF~~ SOA, the vehicle-~~PMF~~ LO-SOA) as constraints based on the same ambient OA datasets as PMF model during the ~~winter/summer~~ observations of Shanghai. Note that in the mass spectra and daily patterns, the OOA PMF factors which compared with vehicle LO-SOA and Cooking SOA respectively are the same, rather than the two resolved factors.

As shown in **Fig.5**, compared with PMF results, the proportions of HOA (7%) and COA (11%) obtained by source apportionment with ME-2 have significantly decreased to the expected value during the winter observation (Huang et al., 2020; Xu et al., 2020). As expected, other POA contributions were identified in the highly polluted season, consistent-correlated well with $C_2H_4O_2^+$ and $C_{10}H_8^+$ influences.

带格式的: 下标
带格式的: 下标
带格式的: 下标
带格式的: 上标
带格式的: 下标
带格式的: 下标
带格式的: 上标

383 ~~which from~~ are well-known fragments from biomass burning and coal combustion emissions (~~Fig.5, Figure~~
384 ~~Fig.S17 and Table S21~~). The diurnal patterns of ~~PMF factors~~HOA_PMF were consistent with ~~and~~
385 HOA_ME-2 factors ~~were consistent with the corresponding tracers~~ during the winter observation, ~~presenting~~
386 low concentration during the daytime and high concentration at nighttime, likely due to the combined
387 influence of boundary layer height and emissions from diesel vehicles during the nighttime. The temporal
388 variation of two HOA factors showed a high correlation with NO_x (Pearson $r > 0.7$), suggesting two HOA
389 factors are associated with vehicle emissions. Some variabilities existed between the diurnal cycle of
390 COA_PMF and COA_ME-2. However, COA_ME-2 correlated better with C₆H₁₀O⁺ than COA_PMF, which
391 was considered a fragment tracer mainly from cooking emissions. For SOA factors, the sum of cooking SOA
392 and vehicle LO-SOA had a high correlation with nitrate (Pearson $r = 0.84$; ~~Fig.S17 and Table S21~~) and
393 fragments of low-oxidizing substances (C₇H₃O⁺; Pearson $r = 0.95$). In addition, ~~We-we~~ noticed that the
394 vehicle SOA analyzed by ME-2 exhibited ~~more consistence~~ consistency with the diurnal variation of nitrate,
395 especially the reasonable morning peak- (~~~09:00~~)~~disappears-retained at night~~, which shows that ~~implying~~
396 ~~that the LO-OOA mixed with POA~~vehicle SOA -is well separated by using ME-2 in winter. MO-OOA
397 resolved via ME-2 was characterized by prominent signal at m/z 28 and m/z 44, consistent with those in
398 OOA identified by using PMF and in other studies (Duan et al., 2020; Kim et al., 2017). ~~Meanwhile, there~~
399 was a strong correlation between MO-OOA time series and sulfate (Pearson $r = 0.93$), which was
400 representative of regional aging species. Unfortunately, the SOA factor corresponding to other-POA (likely
401 biomass burning OA) has not been resolved. Some studies have been found that OA emitted by biomass
402 burning will be rapidly oxidized in the ambient atmosphere, and the BBOA in the fresh plume is mostly
403 aged OA (Zhou et al., 2017). ~~When the aged biomass burning OA is further oxidized, it is difficult to be~~
404 ~~identified the biomass burning SOA from mixed within OOA without constraining its SOA factor.~~ Overall,
405 ME-2 source analysis with the input of four source spectra profiles significantly improved the OA source

带格式的: 字体: 加粗

带格式的: 字体: 加粗

带格式的: 字体: 加粗

带格式的: 下标

带格式的: 下标

带格式的: 上标

带格式的: 字体: 加粗

带格式的: 字体: 加粗, 非突出显示

带格式的: 字体: 加粗

带格式的: 字体: 加粗, 非突出显示

带格式的: 字体: 加粗

406 apportionment during the wintertime. In comparing the ME-2 analysis results with only two POA factors
407 constraining to that of the four factors constraining, the diurnal variations of HOA and COA obtained by
408 constraining two primary sources were more consistent with those of the ME-2 constraint four-factor than
409 PMF. However, OOA and POA were weakly separated, and the diurnal patterns of OOA were correlated
410 with the case for the peak of other-POA during the evening (20:00~21:00) (Figure Fig.S18-S19-). These
411 phenomena imply that the SOA factor constraint can be more environmentally meaningful factors to a
412 certain extent.

413 For the source apportionment in summer with high oxidation conditions (Fig. S8S20), ~~the~~ the fraction of
414 COA reduced from 21% (PMF result) to 12% (ME-2 result). ~~As a primary emission source with a stable~~
415 ~~contribution, COA based on ME-2 analysis accounted for the same proportion of OA in summer as in winter.~~

416 Moreover, the diurnal patterns of ME-2 SOA factors present more reasonable than PMF SOA factors. For
417 example, the MO-OOA obtained based on ME-2 analysis was in good agreement with the diurnal variation
418 of O_x in summer. ~~The~~ The Pearson r between MO-OOA ME-2 and CO₂⁺(m/z 44), a marker of SOA was 0.95,
419 higher than that of MO-OOA PMF (0.79), which better reflects the characteristics of the MO-OOA factor in
420 ME-2 (Fig.S21 and Table S22). In general, the accurate source apportionment results have significantly

421 indicated that the reliability source profiles of the primary and secondary of cooking and vehicles obtained
422 in our study can be used as constraints for source apportionment of OA with ME-2 in various primary
423 emissions or high oxidation conditions.

4. Limitations and future work ~~Conclusions and Implication~~

425 POA emissions, and SOA formation in Go: PAM reactor from urban cooking and vehicular
426 sources ~~lifestyle sources~~ were explored. The aged COA had higher hydrocarbon ions than aged HOA in mass
427 spectra. ~~Based on~~ ~~The~~ ~~mass~~ spectra profiles of ~~these two~~ urban cooking and vehicular sources ~~lifestyle~~
428 ~~sources~~ derived from the lab simulation were performed as constraint, ~~in the~~ ME-2 model ~~source~~

带格式的: 非突出显示

带格式的: 非突出显示

带格式的: 非突出显示

带格式的: 非突出显示

带格式的: 非突出显示

带格式的: 非突出显示

带格式的: 非突出显示

带格式的: 非突出显示

带格式的: 非突出显示

带格式的: 非突出显示

带格式的: 非突出显示

带格式的: 非突出显示

带格式的: 非突出显示

带格式的: 非突出显示

带格式的: 非突出显示

带格式的: 非突出显示

带格式的: 非突出显示

带格式的: 非突出显示

带格式的: 字体: 加粗, 非突出显示

带格式的: 字体: 加粗

带格式的: 非突出显示

带格式的: 非突出显示

带格式的: 非突出显示

带格式的: 非突出显示

带格式的: 下标

带格式的: 上标

带格式的: 字体: 加粗

带格式的: 字体: 加粗

429 ~~apportionment. The OA source apportionment using ME-2 compared with unconstrained PMF is based on~~
430 ~~the HR OA datasets in Shanghai suggest that validated~~ the reasonable of the primary and secondary source
431 profiles of cooking and vehicles ~~were obtained. To our best knowledge, it's the first time to estimate the~~
432 ~~contribution of anthropogenic sources— Chinese cooking SOA and vehicle SOA in ambient air by a~~
433 ~~multilinear engine model (ME 2), through creatively employs mass spectra of SOA factors to constrain the~~
434 ~~OA source apportionments, all which has been implemented in biogenic SOA (Hu et al., 2016b; Zhang et al.,~~
435 ~~2017b). Due to the limitation of research methods, It is noted that the vehicle experiments were solely~~
436 conducted under ~~a single engine with gasoline, and the cooking experiment only related to limited cooking~~
437 ~~styles. The variations of VOCs in diesel and gasoline vehicle emissions may lead to differences in the SOA~~
438 ~~characteristics (Wang et al., 2020). The POA and gas-phase precursor emitted from other cooking styles -~~
439 ~~meat charbroiling can also form a large amount of SOA after photochemical oxidation (Kaltsonoudis et al.,~~
440 ~~2017). More work needs to be done to explore the POA and SOA mass spectrometric characteristics of~~
441 ~~emissions from vehicles and cooking sources. In addition, SOA mass spectra were split from aged COA and~~
442 ~~aged HOA by using the PMF model, and therefore provided limited information on dynamic SOA mass~~
443 ~~spectra: we suggested that further studies control the oxidation conditions to obtain a set of dynamic pure~~
444 ~~SOA spectral profile. Due to the limitation of Go: PAM, dilution and high concentration of OH radicals~~
445 ~~without other inorganic aerosol seeds were adopted to measure and simulate atmospheric aging of aerosols.~~
446 ~~Thus, the possible atmospheric transformations and the reaction pathway are affected. the oxidation~~
447 ~~conditions without other inorganic aerosol seeds. In the future, it is still necessary to take further researches,~~
448 ~~for instance, use a quasi-atmospheric aerosol evolution study (QUALITY) chamber (Guo et al., 2020) to~~
449 ~~study the SOA formation under different actual oxidation conditions, like high/low NO_x and so forth.~~
450 ~~Moreover, ambient datasets obtained from different sites and seasons need to be analyzed to validate the~~
451 ~~application of POA and SOA profiles of cooking and vehicles in this study, noting selecting a loose~~

域代码已更改

带格式的: 非突出显示

452 constraint via a value in SOA factors due to their high variability.

453 ~~In the future, it is still necessary to take further researches, for instance, use a quasi-atmospheric aerosol~~
454 ~~evolution study (QUALITY) chamber to study the SOA formation under different actual oxidation~~
455 ~~conditions, like high/low NO_x and so forth. According to previous studies, using some parameter~~
456 ~~assumptions of vehicle exhaust, it is estimated that cooking SOA accounts for 35% of the SOA in downtown~~
457 ~~Los Angeles through the model.~~ Our research found that SOA from the urban cooking and vehicular sources
458 lifestyle sources contributed 19% and 35% of OA in the wintertime and summertime of Shanghai,
459 implying the need to develop control measures to reduce emissions from cooking and vehicular sources
460 lifestyle sources in the future.

462 Nomenclature table

<u>Abbreviations</u>	<u>Description</u>
<u>OA</u>	<u>organic aerosol</u>
<u>POA</u>	<u>primary organic aerosol</u>
<u>SOA</u>	<u>secondary organic aerosol</u>
<u>HOA</u>	<u>hydrocarbon-like organic aerosol; associated with vehicle-related emissions in urban</u>
<u>COA</u>	<u>cooking organic aerosol</u>
<u>LO-OOA</u>	<u>low oxygenated organic aerosol</u>
<u>MO-OOA</u>	<u>more oxygenated organic aerosol</u>
<u>PMF</u>	<u>positive matrix factorization</u>
<u>ME-2</u>	<u>a multilinear engine</u>
<u>HR-ToF-AMS</u>	<u>high-resolution time-of-flight aerosol mass spectrometer</u>
<u>SMPS</u>	<u>scanning mobility particle sizers</u>
<u>Go: PAM</u>	<u>Gothenburg Potential Aerosol Mass reactor</u>
<u>VOCs</u>	<u>volatile organic compounds</u>
<u>SVOCs</u>	<u>semi-volatile organic compounds</u>
<u>IVOCs</u>	<u>intermediate volatile organic compounds</u>
<u>O-VOCs</u>	<u>oxygenated volatile organic compounds</u>
<u><i>f</i>_{28, 29, 41, 43, ...}</u>	<u>fraction of m/z 28, 29, 41, 43... in total organic aerosol</u>
<u>aged HOA</u>	<u>organic aerosols oxidized by Potential Aerosol Mass reactor in vehicle experiments</u>
<u>aged COA</u>	<u>organic aerosols oxidized by Potential Aerosol Mass reactor in cooking experiments</u>
<u>LO-SOA</u>	<u>low oxidized vehicle secondary organic aerosol</u>

带格式表格

Supporting information

Schematic depiction of the simulation and measurement system (Figure S1); Details of the mass spectra of aged HOA and aged COA (Figures S2-S5; [Table S4-S7](#)); Van Krevelen diagram of POA, aged COA, and aged HOA (Figure S6); [The choice for the PMF and ME-2 analysis \(Figure S7-S10; Table S8-S9; Figure S13-S14; Table S19-S20\)](#); ME-2 source analysis during the summer observation in Shanghai ([Figure S8-S19](#)); [The time-series correlations of factors with external tracers \(Figure S17-S18, S21; Table S21-S22\)](#); Experimental parameters (Table S1-S3); Mass spectra similarity analysis [between mass spectra of ambient factor and mass spectral profiles for vehicle and cooking](#) (Table [S2S14-S4S18](#); Figure [S7S11](#)).

Data availability. The data provided in this paper can be obtained from the author upon request (songguo@pku.edu.cn).

Author contribution. Wenfei Zhu, Zirui Zhang, Hui Wang, Ying Yu, Zheng Chen, Ruizhe Shen, Rui Tan, Kai Song, Kefan Liu, Rongzhi Tang, Yi Liu, Yuanju Li, Wenbin Zhang, and Zhou Zhang conducted the experiments. Wenfei Zhu, Zirui Zhang, Song Guo, and Min Hu analyzed the data. Shengrong Lou, Shijin Shuai, Hongming Xu, Shuangde Li, Yunfa Chen, Francesco Canonaco, and Andre. S. H. Prévôt reviewed and commented on the paper. Wenfei Zhu and Song Guo wrote the paper.

Competing interests. The authors declare no competing financial interest.

Acknowledgments. This research was supported by the National Key R&D Program of China (2016YFC0202000), the National Natural Science Foundation of China (51636003, 41977179, 91844301, and 21677002), Beijing Municipal Science and Technology Commission (Z201100008220011), the Open Research Fund of State Key Laboratory of Multiphase Complex Systems (MPCS-2019-D-09), the Natural Science Foundation of Beijing (8192022), ~~and~~ the fellowship of China Postdoctoral Science Foundation (2020M680242), [and the Open Research Fund of State Key Laboratory of Multiphase Complex Systems](#)

486 [\(No. MPC2021-D-12\)](#).

487 **References**

- 488 Alfarrá, M.R., Prevot, A.S.H., Szidat, S., Sandradewi, J., Weimer, S., Lanz, V.A., Schreiber, D., Mohr, M., Baltensperger, U., 2007.
489 Identification of the mass spectral signature of organic aerosols from wood burning emissions. *Environmental Science &*
490 *Technology* 41, 5770-5777.
- 491 Budisulistiorini, S.H., Canagaratna, M.R., Croteau, P.L., Marth, W.J., Baumann, K., Edgerton, E.S., Shaw, S.L., Knipping, E.M.,
492 Worsnop, D.R., Jayne, J.T., Gold, A., Surratt, J.D., 2013. Real-Time Continuous Characterization of Secondary Organic
493 Aerosol Derived from Isoprene Epoxydiols in Downtown Atlanta, Georgia, Using the Aerodyne Aerosol Chemical Speciation
494 Monitor. *Environmental Science & Technology* 47, 5686-5694.
- 495 Canagaratna, M., Jimenez, J., Kroll, J., Chen, Q., Kessler, S., Massoli, P., Hildebrandt Ruiz, L., Fortner, E., Williams, L., Wilson,
496 K., 2015. Elemental ratios measurements of organic compounds using aerosol mass spectrometry: characterization,
497 improved calibration, and implications. *Atmos. Chem. Phys* 15, 253-272.
- 498 Canagaratna, M.R., Jayne, J.T., Jimenez, J.L., Allan, J.D., Alfarrá, M.R., Zhang, Q., Onasch, T.B., Drewnick, F., Coe, H.,
499 Middlebrook, A., Delia, A., Williams, L.R., Trimborn, A.M., Northway, M.J., DeCarlo, P.F., Kolb, C.E., Davidovits, P., Worsnop,
500 D.R., 2007. Chemical and microphysical characterization of ambient aerosols with the aerodyne aerosol mass spectrometer.
501 *Mass Spectrometry Reviews* 26, 185-222.
- 502 Canonaco, F., Crippa, M., Slowik, J.G., Baltensperger, U., Prevot, A.S.H., 2013. SoFi, an IGOR-based interface for the efficient
503 use of the generalized multilinear engine (ME-2) for the source apportionment: ME-2 application to aerosol mass
504 spectrometer data. *Atmospheric Measurement Techniques* 6, 3649-3661.
- 505 Collier, S., Zhou, S., Kuwayama, T., Forestieri, S., Brady, J., Zhang, M., Kleeman, M., Cappa, C., Bertram, T., Zhang, Q., 2015.
506 Organic PM Emissions from Vehicles: Composition, O/C Ratio, and Dependence on PM Concentration. *Aerosol Science*
507 *and Technology* 49, 86-97.
- 508 Crippa, M., Canonaco, F., Lanz, V.A., Aijala, M., Allan, J.D., Carbone, S., Capes, G., Ceburnis, D., Dall'Osto, M., Day, D.A.,
509 DeCarlo, P.F., Ehn, M., Eriksson, A., Freney, E., Hildebrandt Ruiz, L., Hillamo, R., Jimenez, J.L., Junninen, H., Kiendler-Scharr,
510 A., Kortelainen, A.M., Kulmala, M., Laaksonen, A., Mensah, A., Mohr, C., Nemitz, E., O'Dowd, C., Ovadnevaite, J., Pandis, S.N.,
511 Petaja, T., Poulain, L., Saarikoski, S., Sellegri, K., Swietlicki, E., Tiitta, P., Worsnop, D.R., Baltensperger, U., Prevot, A.S.H., 2014.
512 Organic aerosol components derived from 25 AMS data sets across Europe using a consistent ME-2 based source
513 apportionment approach. *Atmospheric Chemistry and Physics* 14, 6159-6176.
- 514 Duan, J., Huang, R.-J., Li, Y., Chen, Q., Zheng, Y., Chen, Y., Lin, C., Ni, H., Wang, M., Ovadnevaite, J., Ceburnis, D., Chen, C.,
515 Worsnop, D.R., Hoffmann, T., O'Dowd, C., Cao, J., 2020. Summertime and wintertime atmospheric processes of secondary
516 aerosol in Beijing. *Atmospheric Chemistry and Physics* 20, 3793-3807.
- 517 Elser, M., Huang, R.-J., Wolf, R., Slowik, J.G., Wang, Q., Canonaco, F., Li, G., Bozzetti, C., Daellenbach, K.R., Huang, Y., Zhang,
518 R., Li, Z., Cao, J., Baltensperger, U., El-Haddad, I., Prevot, A.S.H., 2016. New insights into PM_{2.5} chemical composition and
519 sources in two major cities in China during extreme haze events using aerosol mass spectrometry. *Atmospheric Chemistry*
520 *and Physics* 16, 3207-3225.
- 521 Ge, X., Li, L., Chen, Y., Chen, H., Wu, D., Wang, J., Xie, X., Ge, S., Ye, Z., Xu, J., 2017. Aerosol characteristics and sources in
522 Yangzhou, China resolved by offline aerosol mass spectrometry and other techniques. *Environmental Pollution* 225, 74-85.
- 523 Gentner, D.R., Harley, R.A., Miller, A.M., Goldstein, A.H., 2009. Diurnal and Seasonal Variability of Gasoline-Related Volatile
524 Organic Compound Emissions in Riverside, California. *Environmental Science & Technology* 43, 4247-4252.
- 525 Guo, S., Hu, M., Guo, Q., Zhang, X., Zheng, M., Zheng, J., Chang, C.C., Schauer, J.J., Zhang, R., 2012. Primary Sources and
526 Secondary Formation of Organic Aerosols in Beijing, China. *Environmental Science & Technology* 46, 9846-9853.
- 527 Guo, S., Hu, M., Peng, J., Wu, Z., Zamora, M.L., Shang, D., Du, Z., Zheng, J., Fang, X., Tang, R., Wu, Y., Zeng, L., Shuai, S.,
528 Zhang, W., Wang, Y., Ji, Y., Li, Y., Zhang, A.L., Wang, W., Zhang, F., Zhao, J., Gong, X., Wang, C., Molina, M.J., Zhang, R., 2020.

529 Remarkable nucleation and growth of ultrafine particles from vehicular exhaust. *Proceedings of the National Academy of*
530 *Sciences of the United States of America* 117, 3427-3432.

531 Guo, S., Hu, M., Zamora, M.L., Peng, J., Shang, D., Zheng, J., Du, Z., Wu, Z., Shao, M., Zeng, L., Molina, M.J., Zhang, R., 2014.
532 Elucidating severe urban haze formation in China. *Proceedings of the National Academy of Sciences of the United States of*
533 *America* 111, 17373-17378.

534 He, L.Y., Huang, X.F., Xue, L., Hu, M., Lin, Y., Zheng, J., Zhang, R., Zhang, Y.H., 2011. Submicron aerosol analysis and organic
535 source apportionment in an urban atmosphere in Pearl River Delta of China using high-resolution aerosol mass
536 spectrometry. *Journal of Geophysical Research Atmospheres* 116, -.

537 He, L.Y., Lin, Y., Huang, X.F., Guo, S., Xue, L., Su, Q., Hu, M., Luan, S.J., Zhang, Y.H., 2010. Characterization of high-resolution
538 aerosol mass spectra of primary organic aerosol emissions from Chinese cooking and biomass burning. *Atmospheric*
539 *Chemistry and Physics* 10, 11535-11543.

540 Hu, W., Hu, M., Hu, W., Jimenez, J.L., Yuan, B., Chen, W., Wang, M., Wu, Y., Chen, C., Wang, Z., 2016a. Chemical composition,
541 sources, and aging process of submicron aerosols in Beijing: Contrast between summer and winter. *Journal of Geophysical*
542 *Research Atmospheres* 121, 1955-1977.

543 Hu, W., Hu, M., Hu, W.W., Zheng, J., Chen, C., Wu, Y., Guo, S., 2017. Seasonal variations in high time-resolved chemical
544 compositions, sources, and evolution of atmospheric submicron aerosols in the megacity Beijing. *Atmospheric Chemistry &*
545 *Physics* 17, 9979-10000.

546 Hu, W., Palm, B.B., Day, D.A., Campuzano-Jost, P., Krechmer, J.E., Peng, Z., de Sa, S.S., Martin, S.T., Alexander, M.L.,
547 Baumann, K., Hacker, L., Kiendler-Scharr, A., Koss, A.R., de Gouw, J.A., Goldstein, A.H., Seco, R., Sjostedt, S.J., Park, J.-H.,
548 Guenther, A.B., Kim, S., Canonaco, F., Prevot, A.S.H., Brune, W.H., Jimenez, J.L., 2016b. Volatility and lifetime against OH
549 heterogeneous reaction of ambient isoprene-epoxydiols-derived secondary organic aerosol (IEPOX-SOA). *Atmospheric*
550 *Chemistry and Physics* 16, 11563-11580.

551 Huang, R.-J., He, Y., Duan, J., Li, Y., Chen, Q., Zheng, Y., Chen, Y., Hu, W., Lin, C., Ni, H., Dai, W., Cao, J., Wu, Y., Zhang, R., Xu,
552 W., Ovadnevaite, J., Ceburnis, D., Hoffmann, T., O'Dowd, C.D., 2020. Contrasting sources and processes of particulate
553 species in haze days with low and high relative humidity in wintertime Beijing. *Atmospheric Chemistry and Physics* 20,
554 9101-9114.

555 Huang, X.F., He, L.Y., Hu, M., Canagaratna, M.R., Kroll, J.H., Ng, N.L., Zhang, Y.H., Lin, Y., Xue, L., Sun, T.L., 2011.
556 Characterization of submicron aerosols at a rural site in Pearl River Delta of China using an Aerodyne High-Resolution
557 Aerosol Mass Spectrometer. *Atmospheric Chemistry & Physics* 11, 1865-1877.

558 Kaltsonoudis, C., Kostenidou, E., Louvaris, E., Psychoudaki, M., Tsiligiannis, E., Florou, K., Liangou, A., Pandis, S.N., 2017.
559 Characterization of fresh and aged organic aerosol emissions from meat charbroiling. *Atmospheric Chemistry and Physics*
560 17, 7143-7155.

561 Katragadda, H.R., Fullana, A., Sidhu, S., Carbonell-Barrachina, A.A., 2010. Emissions of volatile aldehydes from heated
562 cooking oils. *Food Chemistry* 120, 59-65.

563 Kim, H., Zhang, Q., Bae, G.-N., Kim, J.Y., Lee, S.B., 2017. Sources and atmospheric processing of winter aerosols in Seoul,
564 Korea: insights from real-time measurements using a high-resolution aerosol mass spectrometer. *Atmospheric Chemistry*
565 *and Physics* 17, 2009-2033.

566 Klein, F., Platt, S.M., Farren, N.J., Detournay, A., Bruns, E.A., Bozzetti, C., Daellenbach, K.R., Kilic, D., Kumar, N.K., Pieber, S.M.,
567 Slowik, J.G., Temime-Roussel, B., Marchand, N., Hamilton, J.F., Baltensperger, U., Prevot, A.S.H., El Haddad, I., 2016.
568 Characterization of Gas-Phase Organics Using Proton Transfer Reaction Time-of-Flight Mass Spectrometry: Cooking
569 Emissions. *Environmental Science & Technology* 50, 1243-1250.

570 Kostenidou, E., Lee, B.-H., Engelhart, G.J., Pierce, J.R., Pandis, S.N., 2009. Mass Spectra Deconvolution of Low, Medium, and
571 High Volatility Biogenic Secondary Organic Aerosol. *Environmental Science & Technology* 43, 4884-4889.

572 Kroll, J.H., Smith, J.D., Worsnop, D.R., Wilson, K.R., 2012. Characterisation of lightly oxidised organic aerosol formed from
573 the photochemical aging of diesel exhaust particles. *Environmental Chemistry* 9, 211-220.

574 Li, J., Liu, Q., Li, Y., Liu, T., Huang, D., Zheng, J., Zhu, W., Hu, M., Wu, Y., Lou, S., Hallquist, A.M., Hallquist, M., Chan, C.K.,
575 Canonaco, F., Prevot, A.S.H., Fung, J.C.H., Lau, A.K.H., Yu, J.Z., 2019. Characterization of Aerosol Aging Potentials at
576 Suburban Sites in Northern and Southern China Utilizing a Potential Aerosol Mass (Go:PAM) Reactor and an Aerosol Mass
577 Spectrometer. *Journal of Geophysical Research-Atmospheres* 124, 5629-5649.

578 Li, Y.J., Sun, Y., Zhang, Q., Li, X., Li, M., Zhou, Z., Chan, C.K., 2017. Real-time chemical characterization of atmospheric
579 particulate matter in China: A review. *Atmospheric Environment* 158, 270-304.

580 Liu, T., Li, Z., Chan, M., Chan, C.K., 2017. Formation of secondary organic aerosols from gas-phase emissions of heated
581 cooking oils. *Atmospheric Chemistry and Physics* 17, 7333-7344.

582 Liu, T., Wang, Z., Wang, X., Chan, C.K., 2018. Primary and secondary organic aerosol from heated cooking oil emissions.
583 *Atmospheric Chemistry and Physics* 18, 11363-11374.

584 Louvaris, E.E., Karnezi, E., Kostenidou, E., Kaltsonoudis, C., Pandis, S.N., 2017. Estimation of the volatility distribution of
585 organic aerosol combining thermodenuder and isothermal dilution measurements. *Atmospheric Measurement Techniques*
586 10, 3909-3918.

587 Mohr, C., DeCarlo, P.F., Heringa, M.F., Chirico, R., Slowik, J.G., Richter, R., Reche, C., Alastuey, A., Querol, X., Seco, R.,
588 Penuelas, J., Jimenez, J.L., Crippa, M., Zimmermann, R., Baltensperger, U., Prevot, A.S.H., 2012. Identification and
589 quantification of organic aerosol from cooking and other sources in Barcelona using aerosol mass spectrometer data.
590 *Atmospheric Chemistry and Physics* 12, 1649-1665.

591 Ng, N.L., Canagaratna, M.R., Jimenez, J.L., Zhang, Q., Ulbrich, I.M., Worsnop, D.R., 2011. Real-Time Methods for Estimating
592 Organic Component Mass Concentrations from Aerosol Mass Spectrometer Data. *Environmental Science & Technology* 45,
593 910-916.

594 Paatero, P., 1999. The multilinear engine - A table-driven, least squares program for solving multilinear problems,
595 including the n-way parallel factor analysis model. *Journal of Computational and Graphical Statistics* 8, 854-888.

596 Paatero, P., Hopke, P.K., 2003. Discarding or downweighting high-noise variables in factor analytic models. *Analytica*
597 *Chimica Acta* 490, 277-289.

598 Peng, Z., Day, D.A., Ortega, A.M., Palm, B.B., Hu, W., Stark, H., Li, R., Tsigaridis, K., Brune, W.H., Jimenez, J.L., 2016. Non-OH
599 chemistry in oxidation flow reactors for the study of atmospheric chemistry systematically examined by modeling.
600 *Atmospheric Chemistry and Physics* 16, 4283-4305.

601 Presto, A.A., Gordon, T.D., Robinson, A.L., 2014. Primary to secondary organic aerosol: evolution of organic emissions from
602 mobile combustion sources. *Atmospheric Chemistry and Physics* 14, 5015-5036.

603 Qin, Y.M., Tan, H.B., Li, Y.J., Schurman, M.I., Li, F., Canonaco, F., Prevot, A.S.H., Chan, C.K., 2017. Impacts of traffic emissions
604 on atmospheric particulate nitrate and organics at a downwind site on the periphery of Guangzhou, China. *Atmospheric*
605 *Chemistry and Physics* 17, 10245-10258.

606 Reyes-Villegas, E., Green, D.C., Priestman, M., Canonaco, F., Coe, H., Prevot, A.S.H., Allan, J.D., 2016. Organic aerosol source
607 apportionment in London 2013 with ME-2: exploring the solution space with annual and seasonal analysis. *Atmospheric*
608 *Chemistry and Physics* 16, 15545-15559.

609 Robinson, A.L., Donahue, N.M., Shrivastava, M.K., Weitkamp, E.A., Sage, A.M., Grieshop, A.P., Lane, T.E., Pierce, J.R., Pandis,
610 S.N., 2007. Rethinking organic aerosols: Semivolatile emissions and photochemical aging. *Science* 315, 1259-1262.

611 Schauer, J.J., Kleeman, M.J., Cass, G.R., Simoneit, B.R.T., 2002. Measurement of emissions from air pollution sources. 4.
612 C-1-C-27 organic compounds from cooking with seed oils. *Environmental Science & Technology* 36, 567-575.

613 Sun, J., Zhang, Q., Canagaratna, M.R., Zhang, Y., Ng, N.L., Sun, Y., Jayne, J.T., Zhang, X., Zhang, X., Worsnop, D.R., 2010.
614 Highly time- and size-resolved characterization of submicron aerosol particles in Beijing using an Aerodyne Aerosol Mass
615 Spectrometer. *Atmospheric Environment* 44, 131-140.

616 Sun, Y., Du, W., Fu, P., Wang, Q., Li, J., Ge, X., Zhang, Q., Zhu, C., Ren, L., Xu, W., 2016. Primary and secondary aerosols in
617 Beijing in winter: sources, variations and processes. *Atmospheric Chemistry & Physics* 16, 1-41.

618 Sun, Y., Jiang, Q., Wang, Z., Fu, P., Li, J., Yang, T., Yin, Y., 2014. Investigation of the sources and evolution processes of
619 severe haze pollution in Beijing in January 2013. *Journal of Geophysical Research Atmospheres* 119, 4380-4398.

620 Sun, Y., Xu, W., Zhang, Q., Jiang, Q., Canonaco, F., Prévôt, A.S., Fu, P., Li, J., Jayne, J., Worsnop, D.R., 2018. Source
621 apportionment of organic aerosol from two-year highly time-resolved measurements by an aerosol chemical speciation
622 monitor in Beijing, China. *Atmospheric Chemistry and Physics Discussions*, 1-33.

623 Ulbrich, I., Canagaratna, M., Zhang, Q., Worsnop, D., Jimenez, J., 2009. Interpretation of organic components from positive
624 matrix factorization of aerosol mass spectrometric data. *Atmospheric Chemistry & Physics* 9.

625 Wang, H., Xiang, Z., Wang, L., Jing, S., Lou, S., Tao, S., Liu, J., Yu, M., Li, L., Lin, L., Chen, Y., Wiedensohler, A., Chen, C., 2018.
626 Emissions of volatile organic compounds (VOCs) from cooking and their speciation: A case study for Shanghai with
627 implications for China. *Science of the Total Environment* 621, 1300-1309.

628 Wang, J., Ge, X., Chen, Y., Shen, Y., Zhang, Q., Sun, Y., Xu, J., Ge, S., Yu, H., Chen, M., 2016. Highly time-resolved urban
629 aerosol characteristics during springtime in Yangtze River Delta, China: insights from soot particle aerosol mass
630 spectrometry. *Atmospheric Chemistry and Physics* 16, 9109-9127.

631 Wang, M., Li, S., Zhu, R., Zhang, R., Zu, L., Wang, Y., Bao, X., 2020. On-road tailpipe emission characteristics and ozone
632 formation potentials of VOCs from gasoline, diesel and liquefied petroleum gas fueled vehicles. *Atmospheric Environment*
633 223.

634 Wang, Y.C., Huang, R.J., Ni, H.Y., Chen, Y., Wang, Q.Y., Li, G.H., Tie, X.X., Shen, Z.X., Huang, Y., Liu, S.X., Dong, W.M., Xue, P.,
635 Frohlich, R., Canonaco, F., Elser, M., Daellenbach, K.R., Bozzetti, C., Haddad, I.E., Prevot, A.S.H., Canagaratna, M.R., Worsnop,
636 D.R., Cao, J.J., 2017. Chemical composition, sources and secondary processes of aerosols in Baoji city of northwest China.
637 *Atmospheric Environment* 158, 128-137.

638 Watne, A.K., Pschoudaki, M., Ljungstrom, E., Le Breton, M., Hallquist, M., Jerksjö, M., Fallgren, H., Jutterstrom, S., Hallquist,
639 A.M., 2018. Fresh and Oxidized Emissions from In-Use Transit Buses Running on Diesel, Biodiesel, and CNG. *Environmental
640 Science & Technology* 52, 7720-7728.

641 Xu, J., Shi, J., Zhang, Q., Ge, X., Canonaco, F., Prévôt, A.S., Vonwiller, M., Szidat, S., Ge, J., Ma, J., 2016. Wintertime organic
642 and inorganic aerosols in Lanzhou, China: sources, processes, and comparison with the results during summer.
643 *Atmospheric Chemistry and Physics* 16, 14937-14957.

644 Xu, W., Han, T., Wei, D., Wang, Q., Chen, C., Jian, Z., Zhang, Y., Jie, L., Fu, P., Wang, Z., 2017. Effects of Aqueous-phase and
645 Photochemical Processing on Secondary Organic Aerosol Formation and Evolution in Beijing, China. *Environmental
646 Science & Technology* 51, 762.

647 Xu, W., He, Y., Qiu, Y., Chen, C., Xie, C., Lei, L., Li, Z., Sun, J., Li, J., Fu, P., Wang, Z., Worsnop, D., Sun, Y., 2020. Mass spectral
648 characterization of primary emissions and implications in source apportionment of organic aerosol. *Atmospheric
649 Measurement Techniques* 13, 3205-3219.

650 Ying, Y.A.B., Hui, W.A., A, T.W., Kai, S.A., A, T.T., A, Z.W., C, Y.G., A, H.D., A, S.C., D, L.Z.A.B., 2020. Elucidating the importance
651 of semi-volatile organic compounds to secondary organic aerosol formation at a regional site during the EXPLORE-YRD
652 campaign - ScienceDirect. *Atmospheric Environment*.

653 Zhang, Q., Jimenez, J.L., Canagaratna, M.R., Ulbrich, I.M., Ng, N.L., Worsnop, D.R., Sun, Y., 2011. Understanding atmospheric
654 organic aerosols via factor analysis of aerosol mass spectrometry: a review. *Analytical & Bioanalytical Chemistry* 401,
655 3045-3067.

656 Zhang, X., Zhang, Y., Sun, J., Yu, Y., Canonaco, F., Prevot, A.S.H., Li, G., 2017a. Chemical characterization of submicron
657 aerosol particles during wintertime in a northwest city of China using an Aerodyne aerosol mass spectrometry.
658 *Environmental Pollution* 222, 567-582.

659 Zhang, Y., Tang, L., Sun, Y., Favez, O., Canonaco, F., Albinet, A., Couvidat, F., Liu, D., Jayne, J.T., Wang, Z., Croteau, P.L.,
660 Canagaratna, M.R., Zhou, H.-c., Prevot, A.S.H., Worsnop, D.R., 2017b. Limited formation of isoprene epoxydiols-derived
661 secondary organic aerosol under NO_x-rich environments in Eastern China. *Geophysical Research Letters* 44, 2035-2043.

662 Zhang, Y.J., Tang, L.L., Wang, Z., Yu, H.X., Sun, Y.L., Liu, D., Qin, W., Zhang, H.L., Zhou, H.C., 2014. Insights into
663 characteristics, sources and evolution of submicron aerosols during harvest seasons in Yangtze River Delta (YRD) region,
664 China. *Atmospheric Chemistry & Physics* 14, 9109-9154.

665 Zhang, Z., Zhu, W., Hu, M., Wang, H., Chen, Z., Shen, R., Yu, Y., Tan, R., Guo, S., 2020. Secondary Organic Aerosol from
666 Typical Chinese Domestic Cooking Emissions. *Environmental Science & Technology Letters*.

667 Zhou, S., Collier, S., Jaffe, D.A., Briggs, N.L., Hee, J., Sedlacek, A.J., III, Kleinman, L., Onasch, T.B., Zhang, Q., 2017. Regional
668 influence of wildfires on aerosol chemistry in the western US and insights into atmospheric aging of biomass burning
669 organic aerosol. *Atmospheric Chemistry and Physics* 17, 2477-2493.

670 Zhou, W., Wang, Q., Zhao, X., Xu, W., Chen, C., Du, W., Zhao, J., Canonaco, F., Prevot, A.S.H., Fu, P., Wang, Z., Worsnop, D.R.,
671 Sun, Y., 2018. Characterization and source apportionment of organic aerosol at 260 m on a meteorological tower in Beijing,
672 China. *Atmospheric Chemistry and Physics* 18, 3951-3968.

673 Zhu, Q., Huang, X.-F., Cao, L.-M., Wei, L.-T., Zhang, B., He, L.-Y., Elser, M., Canonaco, F., Slowik, J.G., Bozzetti, C., El-Haddad,
674 I., Prevot, A.S.H., 2018. Improved source apportionment of organic aerosols in complex urban air pollution using the
675 multilinear engine (ME-2). *Atmospheric Measurement Techniques* 11, 1049-1060.

676 Zhu, W., Guo, S., Lou, S., Wang, H., Yu, Y., Xu, W., Liu, Y., Cheng, Z., Huang, X., He, L., Zeng, L., Chen, S., Hu, M., 2021a. A
677 novel algorithm to determine the scattering coefficient of ambient organic aerosols. *Environmental Pollution* 270.

678 Zhu, W., Zhou, M., Cheng, Z., Yan, N., Huang, C., Qiao, L., Wang, H., Liu, Y., Lou, S., Guo, S., 2021b. Seasonal variation of
679 aerosol compositions in Shanghai, China: Insights from particle aerosol mass spectrometer observations. *The Science of
680 the total environment* 771, 144948-144948.

681